EARTHQUAKE ENGINEERING AND STRUCTURAL DYNAMICS
Earthquake Engng. Struct. Dyn. **28**, 763–783 (1999)

SLOSHING ANALYSIS OF RECTANGULAR TANKS WITH A SUBMERGED STRUCTURE BY USING SMALL-AMPLITUDE WATER WAVE THEORY

YOUNG-SUN CHOUN[1,*] AND CHUNG-BANG YUN[2]

[1] *Integrated Safety Assessment Team, Korea Atomic Energy Research Institute, Taejon, Korea*
[2] *Department of Civil Engineering, Korea Advanced Institute of Science and Technology, Taejon, Korea*

SUMMARY

A new sloshing analysis method for rectangular tank systems with a submerged structure are proposed by using the velocity potential and the linear water wave theory. The velocity potential functions are obtained by decomposing the surface wave into a wall-induced wave, reflected and transmitted waves, and a scattered wave.

A simplified method using a response spectrum for zero damping is also proposed. The results of the simplified method are in good agreement with those of the analytical method.

The sloshing response of the fluid-structure system is found to be very sensitive to the characteristics of the ground motion and the configuration of the system. Under typical earthquakes, the submerged structure shows a tendency to decrease sloshing amplitude, hydrodynamic pressure, and base shear, while it shows a tendency to increase the overturning moment. For the ground excitation dominated by low-frequency contents, the sloshing response increases significantly and the contribution of the higher sloshing modes increases. Copyright © 1999 John Wiley & Sons, Ltd.

KEY WORDS: sloshing; rectangular tanks; submerged structure; velocity potential; small-amplitude wave; earthquake

INTRODUCTION

Dynamic behaviour of a fluid–structure system has been studied over the past four decades. In liquid storage systems, the sloshing behaviour of the contained liquid and the dynamic analysis of containers considering fluid–structure interaction effects have been major concerns for many engineers and researchers. To understand the dynamic behaviour of liquid storage tanks and to provide proper design codes, many research groups have concentrated their investigations on the seismic behaviours of liquid containers and on the earthquake-resistant design methods of liquid storage tanks.

In spite of the continuous efforts to enhance the performance of liquid containers against seismic loading, many liquid tanks have been severely damaged in major earthquakes all over the

* Correspondence to: Young-Sun Choun, Integrated Safety Assessment Team, Korea Atomic Energy Research Institute, P.O. Box 105, Yusong, Taejon, 305-600 Korea. E-mail: sunchun@nanum.kaeri.re.kr

CCC 0098–8847/99/070763–21$17·50

Received 31 July 1998
Revised 22 December 1998

world, for instance, the 1964 Alaska, the 1971 San Fernando, the 1979 Imperial Valley, the 1983 Coalinga, the 1989 Loma Prieta, the 1992 Landers, and the 1994 Northridge earthquakes in the United States, the 1964 Niigata, the 1978 Miyagi-Ken-Oki, and the 1995 Kobe earthquakes in Japan, the 1981 Central Greece earthquake, the 1972 Managua earthquake in Nicaragua, the 1977 San Juan earthquake in Argentina, etc.[1–8] According to field reports, liquid storage tanks were mainly damaged either by excessive axial compression due to overall bending of the tank shell or by the sloshing of the contained liquid with insufficient freeboard between the liquid surface and the tank roof.[9]

When the equipment or components are submerged in the liquid, the dynamic response of the fluid–structure systems may significantly change. In a spent nuclear fuel storage pool which is a seismic Category I structure in a nuclear power plant, the hydrodynamic pressure exerted on the pool wall and the sloshing wave height of cooling water in the case with spent fuels are different from those in the case without spent fuels. The spent fuel storage pool structure should assure the safety of the stored spent fuels and its structural integrity against design earthquake load. In addition, it should prevent the overflow of contaminated cooling water over the working area by providing sufficient freeboard and should have sufficient water depth to meet radiation shielding conditions. From this point of view, a clear understanding of sloshing characteristics is essential for the determination of the required freeboard, and for the estimation of hydrodynamic pressure on the pool and stored spent fuel.

Although there have been numerous studies on the sloshing behaviour in fluid–structure systems, there are a limited number of studies reported on the sloshing response in a liquid tank with a submerged body or multi-internal bodies.[10–18] Moreover, most of the current sloshing analysis procedures for the fluid–structure system are limited to numerical methods: Finite Element Method (FEM), Boundary Element Method (BEM), Arbitrary Lagrangian–Eulerian Finite Element Method (ALE-FEM), Arbitrary Lagrangian–Eulerian Boundary Element Method (ALE-BEM). Accordingly, the current method requires not only great efforts in obtaining an accurate analytical model, but also a lot of computation time.

This study presents a new analytical method for the two-dimensional sloshing analysis of rectangular liquid storage tanks with a submerged structure by using the velocity potential formulation and the linear water wave theory. The effect of the submerged structure on the sloshing response under seismic loading is discussed. In practical application, one can obtain an approximate solution of the three-dimensional sloshing response by combining the results of two-dimensional analysis for two different tank systems with different dimensions and input motion.

GEOMETRY OF A TANK SYSTEM

A two-dimensional rectangular tank system with a submerged rectangular structure of width $2a$ and height h is under consideration. The width of the tank is L and the fluid is filled up to a height d from the bottom. Figure 1 shows the geometry and the co-ordinate system of the tank system. A Cartesian co-ordinate system (x, z) with the origin at the centre of the base of the submerged structure is used.

It is assumed that the submerged structure is located on the floor at a distance of b and c from the left and right wall of the tank, respectively, and it is totally submerged. The flexibility of the tank walls and submerged structure are neglected because the sloshing frequencies in real storage tanks lie considerably below the natural frequencies of the tank system.[19–21]

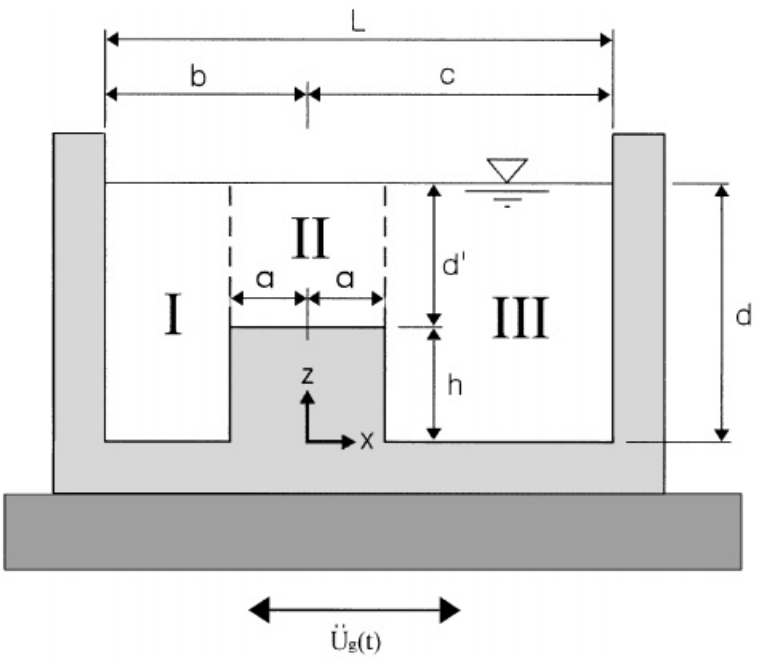

Figure 1. Geometry of a tank system

VELOCITY POTENTIAL FORMULATION

The fluid is assumed to be homogeneous, inviscid, and incompressible, and its motion is assumed to be irrotational. For an irrotational motion, there exists velocity potential, ϕ. The velocity potential function can be found from the continuity equation, the momentum equation, and the boundary conditions. In the (x, z) plane, the continuity equation is expressed in terms of $\phi(x, z, t)$ by Laplace's equation, and the momentum equation is given by the Bernoulli's equation under the assumptions that the flow is irrotational and that the fluid density is invariant. These can be written as

$$\nabla^2\phi(x, z, t) = 0 \tag{1}$$

$$\frac{p}{\rho} + \frac{\partial\phi}{\partial t} + \frac{1}{2}(\nabla\phi \cdot \nabla\phi) + g(z - d) = 0 \tag{2}$$

where ∇^2 is the Laplacian operator, p is the hydrodynamic pressure, ρ is the mass density of fluid, g is the gravitational acceleration, and t is the time.

The solution of Laplace's equation for the rigid tank can be expressed as the sum of an impulsive component, $\phi_i(x, t)$, and a convective component, $\phi_c(x, z, t)$:

$$\phi(x, z, t) = \phi_i(x, t) + \phi_c(x, z, t) \tag{3}$$

The impulsive component satisfies the actual boundary conditions along the tank walls, while the convective component satisfies boundary conditions at the free surface and tank bottom.

The velocity potential $\phi(x, z, t)$ should satisfy Laplace's equation in the fluid domain and the following conditions along the fluid–structure boundaries in the tank system:

$$\frac{\partial \phi}{\partial x} = \dot{u}_g \quad \text{at} \begin{cases} x = -b, & 0 \leqslant z \leqslant d \\ x = c, & 0 \leqslant z \leqslant d \\ |x| = a, & 0 \leqslant z \leqslant h \end{cases} \tag{4}$$

$$\frac{\partial \phi}{\partial z} = 0 \quad \text{at} \begin{cases} -b \leqslant x \leqslant -a, & z = 0 \\ -a \leqslant x \leqslant a, & z = h \\ a \leqslant x \leqslant c, & z = 0 \end{cases} \tag{5}$$

where $\dot{u}_g(t)$ is the horizontal ground velocity. Equation (4) represents the lateral boundary condition along the tank walls and each side of the submerged structure, and equation (5) is the boundary condition along the bottom of the tank and the top of the submerged structure.

Also, the velocity potential should satisfy the kinematic and dynamic boundary conditions at the free surface. In the case of very slow motion, the kinematic and dynamic boundary conditions at the free surface are given as

$$\frac{\partial \phi}{\partial z} = \frac{\partial \eta}{\partial t} \tag{6}$$

$$\frac{\partial \phi}{\partial t} + g\eta = 0 \tag{7}$$

in which $\eta(z, t)$ is the displacement of the free surface about the horizontal plane $z = d$.

The impulsive component of the velocity potential, $\phi_i(x, t)$, can be easily obtained by the Laplace equation (equation (1)) and the lateral boundary condition along the tank walls (equation (4)) as

$$\phi_i(x, t) = (x - e)\dot{u}_g(t) \tag{8}$$

in which e indicates the location of the submerged structure from the centre of the tank given by $e = (c - b)/2$.

If it is assumed that the convective component of the velocity potential, $\phi_c(x, z, t)$, is given by a product of functions for each variable, then Laplace's equation may be solved by the separation of variables method. The convective component of the velocity potential should satisfy the free surface and bottom boundary conditions. To solve the boundary value problem, let the whole fluid domain be divided into three regions as shown in Figure 1, and the convective components of the velocity potential for each region be defined as ϕ_{c1}, ϕ_{c2}, and ϕ_{c3}.

The velocity potentials for the different regions can be expressed as the sum of the propagating mode and the evanescent modes.[22–24] By decomposing the surface waves into wall-induced waves, reflected and transmitted waves by the submerged structure, the general solutions of the time-independent potential function $\varphi(x, z)$ for each fluid region satisfying Laplace's equation and the free surface and bottom boundary conditions can be expressed as

$$\varphi_1(x, z) = \sum_{j=1}^{\infty} \left[\left\{ A_j e^{-ik_j b} e^{-ik_j x} + r_{1j}^{(1)} A_j e^{-ik_j b} e^{ik_j x} + \frac{1}{2} t_{1j}^{s(3)} B_j e^{-ik_j c} \cos k_j(x + l_1) \right. \right.$$
$$\left. \left. + \frac{1}{2} t_{1j}^{a(3)} B_j e^{-ik_j c} \sin k_j(x + l_1) \right\} f_{1j}(z) + \sum_{m=2}^{\infty} \left\{ A_{mj} e^{-ik_j b} e^{-k_{mj} x} + r_{mj}^{(1)} A_j e^{-ik_j b} e^{k_{mj} x} \right.$$

$$+\frac{1}{2}\,t_{mj}^{s(3)}B_j e^{-ik_j c}\cosh k_{mj}(x+l_1)+\frac{1}{2}\,t_{mj}^{a(3)}B_j e^{-ik_j c}\sinh k_{mj}(x+l_1)\Big\}f_{mj}(z)\Big]$$

$$(-b\leqslant x\leqslant -a) \tag{9a}$$

$$\varphi_2(x,z)=\sum_{j=1}^{\infty}\Big\{(C_{1j}\sin k'_j x+D_{1j}\cos k'_j x)g_{1j}(z)+\sum_{n=2}^{\infty}(C_{nj}\sinh k'_{nj}x+D_{nj}\cosh k'_{nj}x)g_{nj}(z)\Big\}$$

$$(-a\leqslant x\leqslant a) \tag{9b}$$

$$\varphi_3(x,z)=\sum_{j=1}^{\infty}\Big[\Big\{B_j e^{-ik_j c}e^{ik_j x}+r_{1j}^{(3)}B_j e^{-ik_j c}e^{-ik_j x}+\frac{1}{2}\,t_{1j}^{s(1)}A_j e^{-ik_j b}\cos k_j(x-l_3)$$

$$+\frac{1}{2}\,t_{1j}^{a(1)}A_j e^{-ik_j b}\sin k_j(x-l_3)\Big\}f_{1j}(z)+\sum_{m=2}^{\infty}\Big\{B_{mj}e^{-ik_j c}e^{k_{mj}x}+r_{mj}^{(3)}B_j e^{-ik_j c}e^{-k_{mj}x}$$

$$+\frac{1}{2}\,t_{mj}^{s(1)}A_j e^{-ik_j b}\cosh k_{mj}(x-l_3)+\frac{1}{2}\,t_{mj}^{a(1)}A_j e^{-ik_j b}\sinh k_{mj}(x-l_3)\Big\}f_{mj}(z)\Big]$$

$$(a\leqslant x\leqslant c) \tag{9c}$$

where

$$l_1=\tfrac{1}{2}(b+a) \tag{10a}$$

$$l_3=\tfrac{1}{2}(c+a) \tag{10b}$$

$$f_{1j}(z)=\left[\frac{d}{2}\left(1+\frac{\sinh 2k_j d}{2k_j d}\right)\right]^{-1/2}\cosh k_j z \tag{11a}$$

$$f_{mj}(z)=\left[\frac{d}{2}\left(1+\frac{\sin 2k_{mj} d}{2k_{mj} d}\right)\right]^{-1/2}\cos k_{mj} z \tag{11b}$$

$$g_{1j}(z)=\left[\frac{d'}{2}\left(1+\frac{\sinh 2k'_j d'}{2k'_j d'}\right)\right]^{-1/2}\cosh k'_j(z-h) \tag{11c}$$

$$g_{nj}(z)=\left[\frac{d'}{2}\left(1+\frac{\sin 2k'_{nj} d'}{2k'_{nj} d'}\right)\right]^{-1/2}\cos k'_{nj}(z-h) \tag{11d}$$

$$\frac{\omega_j^2}{g}=k_j\tanh k_j d=-k_{mj}\tan k_{mj} d$$

$$=k'_j\tanh k'_j d'=-k'_{nj}\tan k'_{nj} d'$$

$$(m,n=2,3,4,\ldots) \tag{12}$$

and $i=\sqrt{-1}$, A_j and B_j are the complex constants associated with the wave amplitudes which are generated by the motions of the left- and right-side walls, respectively; and A_{mj} and B_{mj} are the complex constants associated with the scattered waves. C_{1j}, C_{nj}, D_{1j}, and D_{nj} are the complex constants associated with the transmitted wave amplitudes in region II. $r_{1j}^{(1)}$, $r_{mj}^{(1)}$, $r_{1j}^{(3)}$, and $r_{mj}^{(3)}$ are the complex reflection coefficients for waves on the submerged structure; and $t_{1j}^{s(1)}$, $t_{mj}^{s(1)}$, $t_{1j}^{s(3)}$, $t_{mj}^{s(3)}$, $t_{1j}^{a(1)}$, $t_{mj}^{a(1)}$, $t_{1j}^{a(3)}$, and $t_{mj}^{a(3)}$ are the complex transmission coefficients. Superscripts s and a stand for

the symmetric and antisymmetric parts of the velocity potential; and those of (1) and (3) represent fluid regions I and III, respectively. ω_j is the angular frequencies of the surface waves. k_j and k_{mj} are the wave numbers in fluid regions I and III, while k'_j and k'_{nj} are those in region II. $f_{1j}(z)$ and $f_{mj}(z)$ are orthonormal functions over the interval $(0 \leqslant z \leqslant d)$; and $g_{1j}(z)$ and $g_{nj}(z)$ are orthonormal functions over the interval $(h \leqslant z \leqslant d)$.

In equations (9a) and (9c), the wall-reflected waves of the wave component reflected from the submerged structure are neglected. As a result, the convective components of the velocity potential for each fluid region, $\phi_{ci}(x, z, t)$, can be obtained by

$$\phi_{ci}(x, z, t) = \varphi_i(x, z)\, T(t), \quad i = 1, 2, 3 \tag{13}$$

where $T(t)$ is the function that varies only with time t.

FREE VIBRATION ANALYSIS OF A TANK SYSTEM

Sloshing frequencies of the fluid can be obtained by substituting the time-independent potential $\varphi(x, z)$ expressed as equations (9a)–(9c) into the following lateral boundary condition along two walls of the tank and both sides of the submerged structure:

$$\frac{\partial \phi_c}{\partial x} = 0 \quad \text{at} \quad \begin{cases} x = -b, c, & 0 \leqslant z \leqslant d \\ |x| = a, & 0 \leqslant z \leqslant h \end{cases} \tag{14}$$

By substituting equations (9a) and (9c) into equation (14) and using the orthonormal conditions of $f_{1j}(z)$ and $f_{mj}(z)$, the relations between the wave amplitude coefficients A_j and B_j are obtained. Then, a general expression for the determination of the resonant wave numbers, k_j, can be obtained from the relations between A_j and B_j as

$$\begin{aligned} &(e^{ik_j b} - r_{1j}^{(1)} e^{-ik_j b})(e^{ik_j c} - r_{1j}^{(3)} e^{-ik_j c}) \\ &\quad = -\tfrac{1}{4}(t_{1j}^{s(1)} \sin k_j c_0 - t_{1j}^{a(1)} \cos k_j c_0)(t_{1j}^{s(3)} \sin k_j b_0 + t_{1j}^{a(3)} \cos k_j b_0) \end{aligned} \tag{15}$$

where $b_0 = (b - a)/2$ and $c_0 = (c - a)/2$.

Having required resonant wave numbers k_j from equation (15), the sloshing frequency of the jth mode ω_j (rad/sec) can be calculated from

$$\omega_j = \sqrt{g k_j \tanh k_j d} \tag{16}$$

The jth sloshing mode shape of the free surface, $\psi_j(x)$, can be obtained by substituting B_j into equations (9a)–(9c) and normalizing with the value at the left-side wall:

$$\begin{aligned} \psi_{1j}(x) = \text{Real}\Bigg[&\{(\Omega_{11j}^{(1)} + \Omega_{21j}^{(1)})\cos k_j x - i(\Omega_{11j}^{(1)} - \Omega_{21j}^{(1)})\sin k_j x\} f'_{1j} \\ &+ \sum_{m=2}^{\infty} \{(\Omega_{1mj}^{(1)} + \Omega_{2mj}^{(1)})\cosh k_{mj} x - (\Omega_{1mj}^{(1)} - \Omega_{2mj}^{(1)})\sinh k_{mj} x\} f'_{mj} \Bigg] \\ &(-b \leqslant x \leqslant -a) \end{aligned} \tag{17a}$$

$$\psi_{2j}(x) = \text{Real}\left[\left(C'_{1j}\frac{\sin k'_j x}{\sin k'_j a} + D'_{1j}\frac{\cos k'_j x}{\cos k'_j a}\right)g_{1j}(d) + \sum_{n=2}^{\infty}\left(C'_{nj}\frac{\sinh k'_{nj} x}{\sinh k'_{nj} a} + D'_{nj}\frac{\cos k'_{nj} x}{\cos k'_{nj} a}\right)g_{nj}(d)\right] \quad (-a \leqslant x \leqslant a) \tag{17b}$$

$$\psi_{3j}(x) = \text{Real}\left[\{(\Omega^{(3)}_{11j} + \Omega^{(3)}_{21j})\cos k_j x + \text{i}(\Omega^{(3)}_{11j} - \Omega^{(3)}_{21j})\sin k_j x\} f'_{1j} + \sum_{m=2}^{\infty}\{(\Omega^{(3)}_{1mj} + \Omega^{(3)}_{2mj})\cosh k_{mj} x + (\Omega^{(3)}_{1mj} - \Omega^{(3)}_{2mj})\sinh k_{mj} x\} f'_{mj}\right] \quad (a \leqslant x \leqslant c) \tag{17c}$$

in which

$$\begin{aligned}
\Omega^{(1)}_{11j} &= 1 + \tfrac{1}{4}\kappa_j \,\text{e}^{-\text{i}k_j l_1}(t^{\text{s}(3)}_{1j} + \text{i}t^{\text{a}(3)}_{1j}) \\
\Omega^{(1)}_{21j} &= r^{(1)}_{1j} + \tfrac{1}{4}\kappa_j \,\text{e}^{\text{i}k_j l_1}(t^{\text{s}(3)}_{1j} - \text{i}t^{\text{a}(3)}_{1j}) \\
\Omega^{(1)}_{1mj} &= r^{(1)}_{mj}\,\text{e}^{-2k_{mj}b} + \tfrac{1}{4}\kappa_j \,\text{e}^{-\text{i}k_{mj}(b+b_0)}(t^{\text{s}(3)}_{mj} + t^{\text{a}(3)}_{mj}) \\
\Omega^{(1)}_{2mj} &= r^{(1)}_{mj} + \tfrac{1}{4}\kappa_j \,\text{e}^{k_{mj} l_1}(t^{\text{s}(3)}_{mj} + t^{\text{a}(3)}_{mj}) \\
\Omega^{(3)}_{11j} &= \kappa_j + \tfrac{1}{4}\kappa_j \,\text{e}^{-\text{i}k_j l_3}(t^{\text{s}(1)}_{1j} - \text{i}t^{\text{a}(1)}_{1j}) \\
\Omega^{(3)}_{21j} &= \kappa_j r^{(3)}_{1j} + \tfrac{1}{4}\kappa_j \,\text{e}^{\text{i}k_j l_3}(t^{\text{s}(1)}_{1j} + \text{i}t^{\text{a}(1)}_{1j}) \\
\Omega^{(3)}_{1mj} &= \kappa_j r^{(3)}_{mj}\,\text{e}^{-2k_{mj}c} + \tfrac{1}{4}\,\text{e}^{-\text{i}k_{mj}(c+c_0)}(t^{\text{s}(1)}_{mj} - t^{\text{a}(1)}_{mj}) \\
\Omega^{(3)}_{2mj} &= \kappa_j r^{(3)}_{mj} + \tfrac{1}{4}\kappa_j \,\text{e}^{k_{mj} l_3}(t^{\text{s}(1)}_{mj} - t^{\text{a}(1)}_{mj})
\end{aligned} \tag{18}$$

and $f'_{1j} = f_{1j}(d)/\varphi_{0j}$, $f'_{mj} = f_{mj}(d)/\varphi_{0j}$, $\varphi_{0j} \equiv \varphi_{1j}(-b, d)$, and

$$\kappa_j = \text{i}\,\frac{2\text{e}^{\text{i}k_j b}(1 - r^{(1)}_{1j}\,\text{e}^{-2\text{i}k_j b})}{t^{\text{s}(3)}_{1j}\sin k_j b_0 + t^{\text{a}(3)}_{1j}\cos k_j b_0} \tag{19}$$

The sloshing mode shapes for the three different fluid regions, ψ_{1j}, ψ_{2j}, and ψ_{3j}, should be continuous at $x = -a$ and $x = a$. The continuity conditions at the fluid boundaries are given as

$$\psi_{1j} = \psi_{2j},\ \frac{\text{d}\psi_{1j}}{\text{d}x} = \frac{\text{d}\psi_{2j}}{\text{d}x} \quad \text{at } x = -a \tag{20a}$$

$$\psi_{3j} = \psi_{2j},\ \frac{\text{d}\psi_{3j}}{\text{d}x} = \frac{\text{d}\psi_{2j}}{\text{d}x} \quad \text{at } x = a \tag{20b}$$

Substituting equations (17a)–(17c) into the above continuity conditions, the following are obtained:

$$\begin{bmatrix} -1 & 1 \\ k'_j\cot k'_j a & k'_j\tan k'_j a \\ 1 & 1 \\ k'_j\cot k'_j a & -k'_j\tan k'_j a \end{bmatrix}\begin{Bmatrix} C'_{1j} \\ D'_{1j} \end{Bmatrix} = \begin{Bmatrix} \Lambda_{11j} \\ \Lambda_{12j} \\ \Lambda_{13j} \\ \Lambda_{14j} \end{Bmatrix} \tag{21a}$$

$$\begin{bmatrix} -1 & 1 \\ k'_{nj}\coth k'_{nj}a & -k'_{nj}\tanh k'_{nj}a \\ 1 & 1 \\ k'_{nj}\coth k'_{nj}a & k'_{nj}\tanh k'_{nj}a \end{bmatrix} \begin{Bmatrix} C'_{nj} \\ D'_{nj} \end{Bmatrix} = \begin{Bmatrix} \Lambda_{n1j} \\ \Lambda_{n2j} \\ \Lambda_{n3j} \\ \Lambda_{n4j} \end{Bmatrix}, \quad n = 2, 3, \ldots \tag{21b}$$

in which Λ_{nij} ($n = 1, 2, 3, \ldots$ and $i = 1, \ldots, 4$) are represented by equations (37)–(40) in Appendix I. From equations (21a) and (21b), the unknown coefficients C'_{1j}, C'_{nj}, D'_{1j}, and D'_{nj} in equation (17b) can be determined.

Finally, the sloshing frequencies and sloshing mode shapes will be obtained by substituting reflection and transmission coefficients for surface waves due to the existence of the submerged structure. In determining the reflection and transmission coefficients, it is convenient to decompose the velocity potentials according to the direction of the incident waves.

The reflection and transmission coefficients can be evaluated using the lateral boundary condition (equation (14)) and the continuity conditions of mass and energy flux over the interval ($h \leqslant z \leqslant d$) at $x = -a$ and $x = a$. As a result, the reflection and transmission coefficients for the incident waves of angular frequency ω_j can be determined by[25]

$$\begin{aligned} r_{1j}^{(1)} &= \tfrac{1}{4}(\chi_{1j}^{\mathrm{a}(1)} + \chi_{(m+1)j}^{\mathrm{a}(1)} + \chi_{1j}^{\mathrm{s}(1)} + \chi_{(m+1)j}^{\mathrm{s}(1)})\,\mathrm{e}^{2\mathrm{i}k_j a} \\ t_{1j}^{\mathrm{a}(1)} &= \frac{\chi_{1j}^{\mathrm{a}(1)} - \chi_{(m+1)j}^{\mathrm{a}(1)}}{2\sin k_j c_0}\,\mathrm{e}^{\mathrm{i}k_j a} \\ t_{1j}^{\mathrm{s}(1)} &= \frac{\chi_{1j}^{\mathrm{s}(1)} - \chi_{(m+1)j}^{\mathrm{s}(1)}}{2\cos k_j c_0}\,\mathrm{e}^{\mathrm{i}k_j a} \end{aligned} \tag{22}$$

$$\begin{aligned} r_{1j}^{(3)} &= \tfrac{1}{4}(\chi_{1j}^{\mathrm{a}(3)} + \chi_{(m+1)j}^{\mathrm{a}(3)} + \chi_{1j}^{\mathrm{s}(3)} + \chi_{(m+1)j}^{\mathrm{s}(3)})\,\mathrm{e}^{2\mathrm{i}k_j a} \\ t_{1j}^{\mathrm{a}(3)} &= \frac{\chi_{1j}^{\mathrm{a}(3)} - \chi_{(m+1)j}^{\mathrm{a}(3)}}{2\sin k_j b_0}\,\mathrm{e}^{\mathrm{i}k_j a} \\ t_{1j}^{\mathrm{s}(3)} &= \frac{\chi_{1j}^{\mathrm{s}(3)} - \chi_{(m+1)j}^{\mathrm{s}(3)}}{2\cos k_j b_0}\,\mathrm{e}^{\mathrm{i}k_j a} \end{aligned} \tag{23}$$

The reflection and transmission coefficient vectors for the antisymmetric and symmetric parts of the velocity potential can be obtained by

$$X_{\mathrm{a}j}^{(1)} = U_{\mathrm{a}j}^{(1)^{-1}} \cdot V_{\mathrm{a}j}^{(1)} \tag{24a}$$

$$X_{\mathrm{s}j}^{(1)} = U_{\mathrm{s}j}^{(1)^{-1}} \cdot V_{\mathrm{s}j}^{(1)} \tag{24b}$$

$$X_{\mathrm{a}j}^{(3)} = U_{\mathrm{a}j}^{(3)^{-1}} \cdot V_{\mathrm{a}j}^{(3)} \tag{24c}$$

$$X_{\mathrm{s}j}^{(3)} = U_{\mathrm{s}j}^{(3)^{-1}} \cdot V_{\mathrm{s}j}^{(3)} \tag{24d}$$

where

$$X_{\mathrm{a}j}^{(1)} = \langle \chi_{1j}^{\mathrm{a}(1)} \;\; \chi_{2j}^{\mathrm{a}(1)} \;\; \cdots \;\; \chi_{(m+1)j}^{\mathrm{a}(1)} \;\; \chi_{(m+2)j}^{\mathrm{a}(1)} \;\; \cdots \;\; \chi_{2mj}^{\mathrm{a}(1)} \rangle^{\mathrm{T}} \tag{25a}$$

$$X_{\mathrm{s}j}^{(1)} = \langle \chi_{1j}^{\mathrm{s}(1)} \;\; \chi_{2j}^{\mathrm{s}(1)} \;\; \cdots \;\; \chi_{(m+1)j}^{\mathrm{s}(1)} \;\; \chi_{(m+2)j}^{\mathrm{s}(1)} \;\; \cdots \;\; \chi_{2mj}^{\mathrm{s}(1)} \rangle^{\mathrm{T}} \tag{25b}$$

$$X_{\mathrm{a}j}^{(3)} = \langle \chi_{1j}^{\mathrm{a}(3)} \;\; \chi_{2j}^{\mathrm{a}(3)} \;\; \cdots \;\; \chi_{(m+1)j}^{\mathrm{a}(3)} \;\; \chi_{(m+2)j}^{\mathrm{a}(3)} \;\; \cdots \;\; \chi_{2mj}^{\mathrm{a}(3)} \rangle^{\mathrm{T}} \tag{25c}$$

$$X_{\mathrm{s}j}^{(3)} = \langle \chi_{1j}^{\mathrm{s}(3)} \;\; \chi_{2j}^{\mathrm{s}(3)} \;\; \cdots \;\; \chi_{(m+1)j}^{\mathrm{s}(3)} \;\; \chi_{(m+2)j}^{\mathrm{s}(3)} \;\; \cdots \;\; \chi_{2mj}^{\mathrm{s}(3)} \rangle^{\mathrm{T}} \tag{25d}$$

and $U_{aj}^{(1)}$, $U_{sj}^{(1)}$, $U_{aj}^{(3)}$, and $U_{sj}^{(3)}$, $V_{aj}^{(1)}$, $V_{sj}^{(1)}$, $V_{aj}^{(3)}$, and $V_{sj}^{(3)}$ are vectors and matrices associated with the reflection and transmission coefficients, which are shown in Appendix II.

DYNAMIC ANALYSIS METHODS OF A TANK SYSTEM

The velocity potential function can be expressed as the sum of the impulsive component and the convective component:

$$\phi(x, z, t) = (x - e)\dot{u}_g(t) + \sum_{j=1}^{\infty} \dot{G}_j(t)\psi_j(x)F_j(z) \tag{26}$$

in which $\dot{G}_j(t)$ represents the derivative of $G_j(t)$, the time-dependent function associated with surface wave amplitude, with respect to time which can be determined from the equation of motion, $\psi_j(x)$ is the sloshing mode shape expressed as equations (17a)–(17c), and $F_j(z)$ is identical to $f_{1j}(z)$ in equation (11a).

Substituting equation (26) into the kinematic and dynamic boundary conditions at the free surface and by applying orthogonality condition of $\psi_j(x)$, the equation of motion for a damped system can be derived as

$$\ddot{G}_j(t) + 2\xi_j\omega_j\dot{G}_j(t) + \omega_j^2 G_j(t) = -\frac{\Gamma_j}{F_j(d)}\ddot{u}_g(t) \tag{27}$$

in which ξ_j is the modal damping ratio and Γ_j is the modal participation factor expressed as

$$\Gamma_j = \frac{\int_{-b}^{c}(x - e)\psi_j(x)\,dx}{\int_{-b}^{c}\psi_j^2(x)\,dx} \tag{28}$$

Since the antisymmetric sloshing modes are concerned with the horizontal input motion, only the odd modes ($j = 1, 3, 5, \ldots$) are considered in the sloshing analysis under the horizontal ground acceleration $\ddot{u}_g(t)$.

The solution of the equation of motion for $G_j(t)$ gives

$$G_j(t) = -\frac{\Gamma_j}{\omega_{Dj}F_j(d)}\int_0^t \ddot{u}_g(\tau)\,e^{-\xi_j\omega_j(t-\tau)}\sin\omega_{Dj}(t - \tau)\,d\tau \tag{29}$$

in which ω_{Dj} is the jth angular frequency of the damped system given by $\omega_{Dj} = \omega_j\sqrt{1 - \xi_j^2}$.

Finally, the amplitude of the free surface, $\eta(x, t)$, considering the viscosity of the fluid can be obtained from the dynamic boundary condition at the free surface:

$$\eta(x, t) = -\frac{1}{g}\left[(x - e)\ddot{u}_g(t) + \sum_{j=1}^{\infty}\ddot{G}_j(t)\psi_j(x)F_j(d)\right] \tag{30}$$

The kinematic boundary condition gives another expression for the amplitude of the free surface as

$$\eta(x, t) = -\frac{1}{g}\sum_{j=1}^{\infty}\frac{\omega_j^2}{\omega_{Dj}}\Gamma_j\psi_j(x)\int_0^t \ddot{u}_g(\tau)\,e^{-\xi_j\omega_j(t-\tau)}\sin\omega_{Dj}(t - \tau)\,d\tau \tag{31}$$

When the damping ratio is so small, since the angular frequency of the damped system can be equalized to that of the undamped system, the maximum amplitude for the jth sloshing mode can be obtained by a simplified method as

$$|\eta_{j,\max}(x)| = \frac{1}{g}\,\Gamma_j \psi_j(x) S_{aj}(\xi_j, \omega_j) \tag{32}$$

in which $S_{aj}(\xi_j, \omega_j)$ is the spectral acceleration corresponding to the sloshing frequency ω_j and defined as[26]

$$S_{aj}(\xi_j, \omega_j) \equiv \left[\omega_j \int_0^t \ddot{u}_g(\tau)\, e^{-\xi_j \omega_j (t-\tau)} \sin \omega_j (t-\tau)\, d\tau \right]_{\max} \tag{33}$$

The maximum total sloshing amplitude can be obtained approximately by the Square Root of the Sum of the Squares (SRSS) of the modal values, because the maximum value in each mode does not occur simultaneously.

The pressure induced by the excited fluid can be obtained from the linearized Bernoulli's equation:

$$p(x, z, t) = -\rho \frac{\partial \phi}{\partial t}(x, z, t) - \rho g (z - d) \tag{34}$$

The total shear force at the base of the tank at a given time t_0 can be obtained by integrating the pressure along the two side-walls and both sides of the submerged structure:

$$\begin{aligned} Q(t_0) = &\int_0^{d+\eta(-b,t_0)} p(-b, z, t_0)\, dz - \int_0^{d+\eta(c,t_0)} p(c, z, t_0)\, dz \\ &- \int_0^h p(-a, z, t_0)\, dz + \int_0^h p(a, z, t_0)\, dz \end{aligned} \tag{35}$$

Similarly, the overturning moment can be evaluated from

$$\begin{aligned} M(t_0) = &- \int_0^{d+\eta(-b,t_0)} z p(-b, z, t_0)\, dz + \int_0^{d+\eta(c,t_0)} z p(c, z, t_0)\, dz \\ &+ \int_0^h z p(-a, z, t_0)\, dz - \int_0^h z p(a, z, t_0)\, dz + \int_{-b}^{-a} (x - e)\, p(x, 0, t)\, dx \\ &+ \int_{-a}^{a} (x - e)\, p(x, h, t)\, dx + \int_a^c (x - e) p(x, 0, t)\, dx \end{aligned} \tag{36}$$

SEISMIC RESPONSES

The sloshing response in a fluid–structure system for an earthquake is very sensitive to the frequency characteristics of the system and input motion. Simply speaking, the sloshing response is significant for the resonant frequency, whereas slight for the non-resonant frequency. For an identical fluid storage tank, the sloshing amplitudes may vary from just a few centimetres to

several metres depending on the relationship between the sloshing frequencies and frequency contents of the ground motion.

Typical earthquake accelerations have dominant frequencies of about 1–10 Hz. Therefore, the sloshing response is not significant in typical earthquakes because the sloshing frequencies in tanks are considerably low. For tanks with a submerged structure, in general, the sloshing response decreases with the height of the submerged structure during typical earthquakes because the sloshing frequencies decrease with the height of the submerged structure.[25] However, in an earthquake dominated by low frequencies, the sloshing response will increase significantly, especially, in the tanks with a submerged structure. This implies that the sloshing responses mainly depend upon the relationship between the sloshing frequencies and frequency contents of the ground motion more than the existence of a submerged structure.

This study investigates the sloshing response in a tank system with a submerged structure during several major earthquakes with different frequency characteristics. A tank system with a bottom width of 10 m and water depth of 5 m is considered. A rigid structure with a width of 2 m is assumed to be located on the centre of the tank floor because the effect of the location of the submerged structure on the sloshing frequency is found to be less significant than the height.

For seismic analysis, NS and EW components of the 1940 El Centro, the 1985 Mexico City SCT1, and the 1989 Loma Prieta earthquakes are selected as input ground motions. All the selected earthquake records are scaled with the peak acceleration of $0{\cdot}2g$ for easy comparison of the sloshing responses under the various ground motions.

The sloshing frequencies for the antisymmetric mode in the assumed tank system are listed in Table I. The sloshing frequency decreases due to the existence of the submerged structure as shown in the table. Note that the fundamental sloshing frequency decreases significantly as the submerged structure becomes high.

The peak wave amplitudes for the selected earthquakes are listed in Table II. Modal damping ratios of 0·005 and zero are used for the time history and response spectrum analyses, respectively. Ten sloshing modes are taken in both analyses. The values in parentheses indicate the maximum amplitudes for the first sloshing mode only.

Table II indicates that the response spectrum analysis method with zero damping can be used as a simplified method to determine the sloshing response. In the case without a submerged structure the results of the simplified method are conservative, while in the case with a submerged structure the results are not always conservative. However, since the discrepancies between the results from the two methods are within about 10 per cent, except for the Mexico earthquake, the simplified method may be used for the sloshing analysis in the tank system with the submerged structure.

The peak wave amplitude varies significantly with the size of the submerged structure, and with the characteristics of ground motion in an identical tank as shown in Table II. The peak wave amplitudes tend to decrease as the height of the submerged structure increases. However, it is noticeable that the wave amplitude increases as the height of the submerged structure increases to $h/d = 0{\cdot}5$ under NS component of the El Centro earthquake and the Loma Prieta earthquake.

The height of the submerged structure and the characteristics of input motion also influence the contribution of the fundamental sloshing mode. It is found from the table that the increase of the height of the submerged structure tends to increase the contribution of the fundamental mode slightly, but this tendency may vary with the size and location of the submerged structure and the frequency contents of the input motion. It is also found that if the ground motion is dominated by a low frequency, the contribution of the fundamental mode decreases significantly. For instance,

Table I. Sloshing frequencies (Hz) for various heights (h/d) of a submerged structure

Mode	Height (h/d)		
	0	0·5	0·8
1	0·2675	0·2368	0·1762
2	0·4838	0·4830	0·4720
3	0·6247	0·6246	0·6205
4	0·7391	0·7391	0·7374
5	0·8381	0·8381	0·8374
6	0·9265	0·9265	0·9263
7	1·0072	1·0072	1·0072

Table II. Peak wave amplitudes (cm) for various heights (h/d) of the submerged structure to different earthquakes

Earthquake record	Time history analysis			Response spectrum analysis		
	$h/d = 0$	0·5	0·8	$h/d = 0$	0·5	0·8
El Centro, NS	14·0	18·6	14·1	18·4 (15·1)	17·0 (13·6)	12·8 (11·8)
El Centro, EW	50·0	49·5	48·7	51·4 (46·3)	52·7 (48·1)	47·4 (46·7)
Mexico City	165·1	159·8	31·0	204·9 (89·0)	189·0 (83·9)	34·4 (23·4)
Loma Prieta	80·9	83·2	37·6	87·4 (83·9)	91·1 (88·0)	33·4 (31·9)

Note: The values in parentheses indicate the maximum amplitudes for the first sloshing mode only

the contribution of the fundamental mode is just 43 per cent for $h/d = 0$ and 68 per cent for $h/d = 0{\cdot}8$ during the Mexico City earthquake, because the second sloshing frequency 0·4838 Hz for $h/d = 0{\cdot}0$ is close to the dominant frequency of 0·4883 Hz during the Mexico City earthquake. This indicates that the fundamental mode is not always dominant, hence sufficient higher modes have to be taken into account in the analysis, especially, for the input motion with low-frequency contents. In this example, at least two sloshing modes should be considered in order to obtain good results.

Figures 2 and 3 show the surface wave amplitudes at $x = -b$ for various heights of the submerged structure under the EW component of the El Centro earthquake and the Mexico City earthquake, respectively. Significant changes are given to the waveform by increasing the height of the submerged structure. When the submerged structure is higher, the sloshing period becomes longer and higher sloshing modes appear in the sloshing response as shown in Figure 2(d). The peak value does not always occur at identical times and the peak value does not always coincide with peak ground acceleration. The peak value may have occurred in the low-intensity range and after termination of ground excitation as shown in Figure 2(c) and (d).

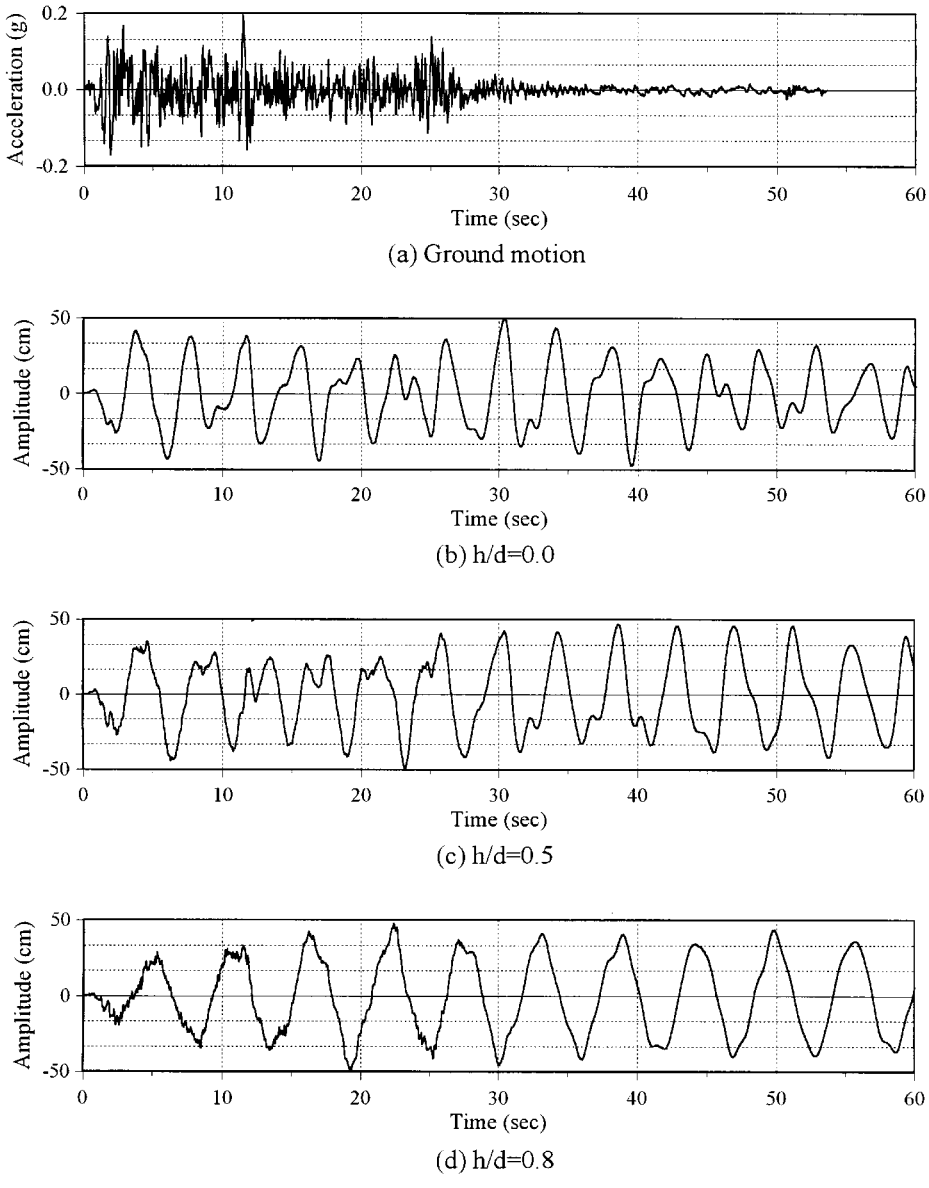

Figure 2. Surface wave amplitudes at $x = -b$ for various heights of the submerged structure during the EW component of the El Centro earthquake

Figure 3 shows that the surface wave amplitude decreases significantly when $h/d = 0{\cdot}8$. The reason is that the second sloshing frequency in the tank system decreases to 0·4720 Hz from 0·4838 Hz as the height of the submerged structure (h/d) increases to 0·8 as shown in Table I. The reduced sloshing frequency is away from the dominant frequency of the Mexico City earthquake 0·4883 Hz and reduces the sloshing response significantly.

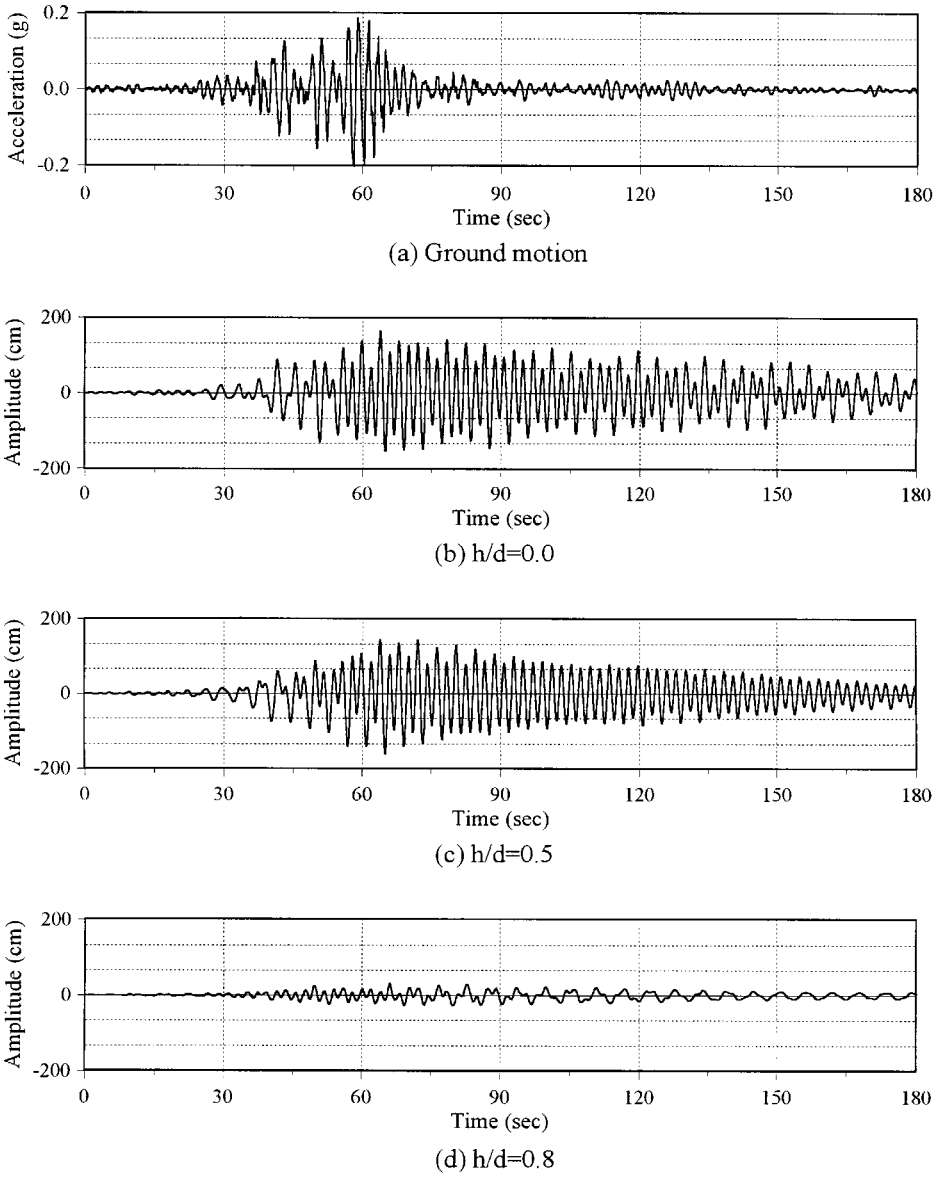

Figure 3. Surface wave amplitudes at $x = -b$ for various heights of the submerged structure during the Mexico City earthquake

The maximum hydrodynamic pressure, which is induced by the free surface displacement of fluid, exerted on the wall of the tank system varies remarkably with the characteristics of ground motion as summarized in Table III. For example, when $h/d = 0$, the hydrodynamic pressure induced by the Mexico City earthquake is about 12 times of that by the NS component of the El Centro earthquake at the mean water level. It is found from the table that the surface wave

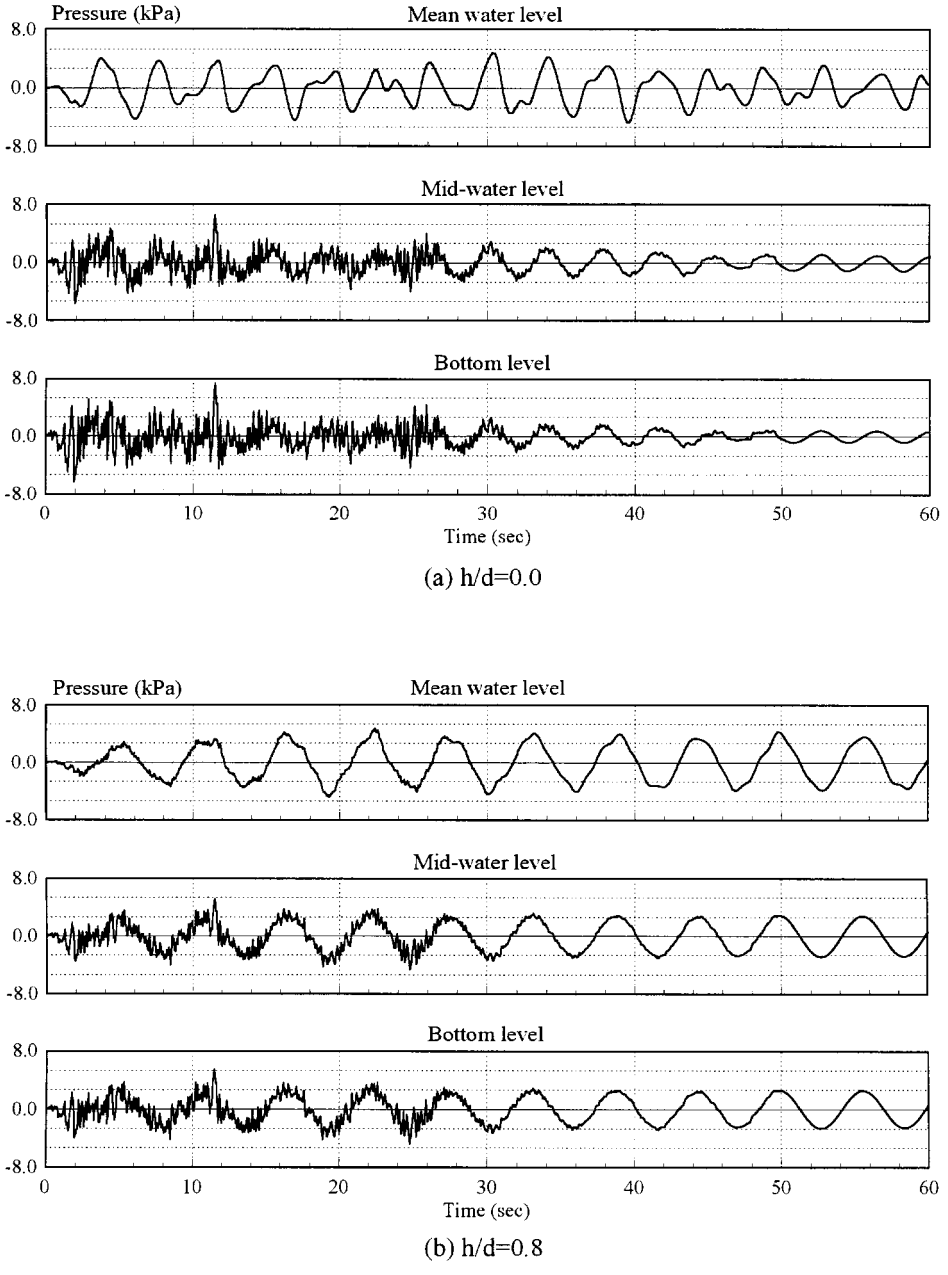

Figure 4. Hydrodynamic pressures at $x = -b$ for various heights of the submerged structure during the EW component of the El Centro earthquake

motion influences the pressure at the bottom level because the fluid participates in the sloshing motion. It is also found that the hydrodynamic pressure tends to decrease as the height of the submerged structure increases.

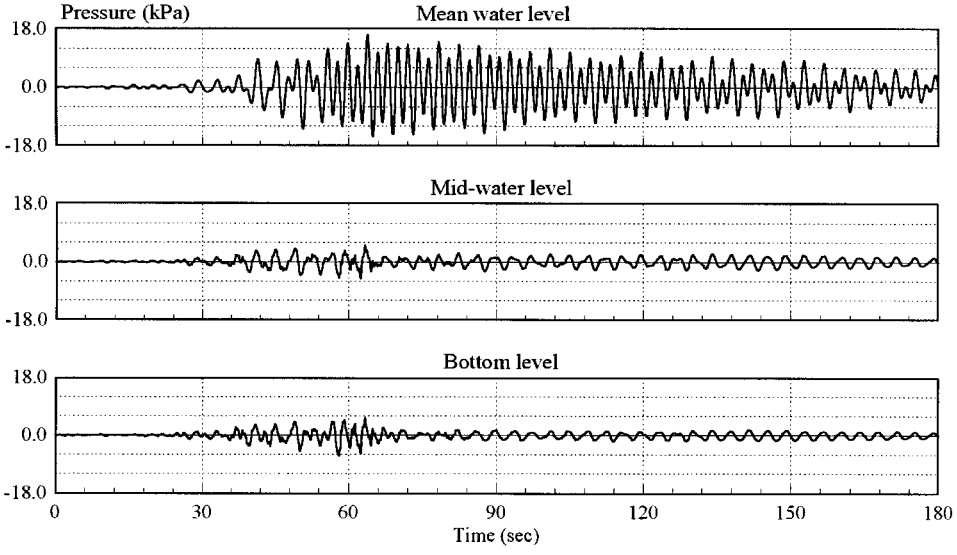

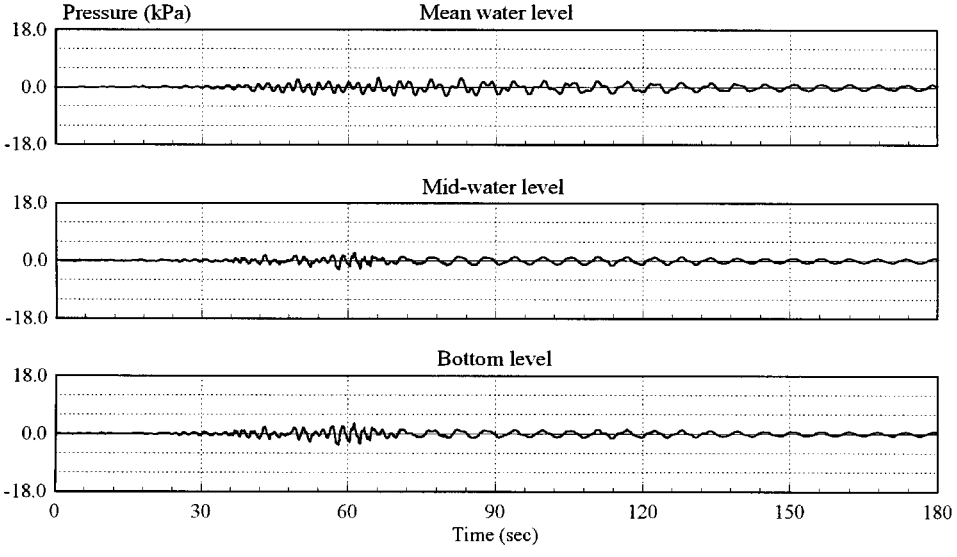

Figure 5. Hydrodynamic pressures at $x = -b$ for various heights of the submerged structure during the Mexico City earthquake

It is observed from Figures 4 and 5 that the convective component of hydrodynamic pressure governs the mean water level, while the impulsive component governs the lower level. It is confirmed from Figure 4 that the surface wave motion influences the pressure at the bottom level.

Table III. Maximum hydrodynamic pressures (kPa) on the wall for various heights (h/d) of the submerged structure

Earthquake record	Mean water level			Bottom level		
	$h/d = 0$	0·5	0·8	$h/d = 0$	0·5	0·8
El Centro, NS	1·37	1·82	1·38	6·83	5·71	4·11
El Centro, EW	4·90	4·85	4·78	7·34	5·39	5·49
Mexico City	16·19	15·67	3·04	6·41	5·76	3·49
Loma Prieta	7·93	8·16	3·70	6·21	5·65	4·17

Table IV. Maximum base shears and overturning moments for various heights (h/d) of the submerged structure

Earthquake record	Base shear (kN) $\lvert Q_{\max}\rvert$			Overturning moment (kN m) $\lvert M_{\max}\rvert$		
	$h/d = 0$	0·5	0·8	$h/d = 0$	0·5	0·8
El Centro, NS	51·7	38·1	32·6	209·6	339·8	297·0
El Centro, EW	61·6	39·4	45·1	251·3	351·6	356·3
Mexico City	113·2	74·3	24·6	628·2	569·8	262·1
Loma Prieta	52·5	45·1	32·9	219·3	378·1	314·4

When $h/d = 0{\cdot}8$, the effect of the surface motion on the pressure at the bottom level increases because the wave length becomes longer due to the decrease in wave number. Figure 4 also shows that the hydrodynamic pressure comes from the sloshing of fluid after the termination of ground acceleration.

The hydrodynamic pressure for the Mexico City earthquake is shown in Figure 5. When $h/d = 0{\cdot}0$, the contribution of the fundamental mode is so low that the pressure at the mean water level is significant but small at the bottom level. Also shown is that the impulsive component of pressure governs at the lower level.

The maximum base shears and overturning moments for various heights (h/d) of the submerged structure are shown in Table IV. The base shear tends to decrease with an increase in the height of the submerged structure except for the El Centro EW earthquake. The maximum values of base shear and overturning moment for the Mexico City earthquake are greater than those for others upto 3 times for $h/d = 0$ and 0·5. This indicates that the low-frequency contents of ground motion increase the sloshing response significantly. For $h/d = 0{\cdot}5$ and 0·8, the base shear shows a tendency to decrease except for the El Centro EW earthquake, while the overturning moment shows a tendency to increase except for the Mexico earthquake.

CONCLUSION

A new sloshing analysis method for rectangular tank systems with a submerged structure for seismic loading is developed by using the velocity potential and the linear water wave theory.

A surface wave is decomposed into a wall-induced wave, reflected and transmitted waves, and a scattered wave, and then the method of separation of variables is used for obtaining velocity potential functions. The reflection and transmission coefficients for the submerged structure are determined by the continuity conditions of mass and energy flux along the common vertical boundaries of the continuous fluid regions and by the lateral boundary conditions along each side of the submerged structure.

A simplified method using a response spectrum for zero damping is also proposed. The results of the simplified method are in fairly good agreement with those of the analytical method.

The sloshing response of the fluid–structure system is found to be very sensitive to the characteristics of the ground motion and the configuration of the system. Under typical earthquakes, the submerged structure shows a tendency to decrease sloshing amplitude, hydrodynamic pressure, and base shear, while it shows a tendency to increase the overturning moment. For the ground excitation dominated by low-frequency contents, the sloshing response increases significantly and the contribution of the higher sloshing modes increases. In this case, sufficient higher modes are to be taken into account in the analysis.

APPENDIX I

Λ_{nij} in equations (21a) and (21b) are expressed as

$$\Lambda_{n1j} = \varphi_{0j}^{-1}\left[\{(\Omega_{11j}^{(1)} + \Omega_{21j}^{(1)})\cos k_j a + (\Omega_{11j}^{(1)} - \Omega_{21j}^{(1)})\sin k_j a\}\psi_{1nj} + \sum_{m=2}^{\infty}\{(\Omega_{1mj}^{(1)} + \Omega_{2mj}^{(1)})\cosh k_{mj} a + (\Omega_{1mj}^{(1)} - \Omega_{2mj}^{(1)})\sinh k_{mj} a\}\psi_{mnj}\right] \tag{37}$$

$$\Lambda_{n2j} = \varphi_{0j}^{-1}\left[k_j\{(\Omega_{11j}^{(1)} + \Omega_{21j}^{(1)})\sin k_j a - (\Omega_{11j}^{(1)} - \Omega_{21j}^{(1)})\cos k_j a\}\psi_{1nj} - \sum_{m=2}^{\infty} k_{mj}\{(\Omega_{1mj}^{(1)} + \Omega_{2mj}^{(1)})\sinh k_{mj} a + (\Omega_{1mj}^{(1)} - \Omega_{2mj}^{(1)})\cosh k_{mj} a\}\psi_{mnj}\right] \tag{38}$$

$$\Lambda_{n3j} = \varphi_{0j}^{-1}\left[\{(\Omega_{11j}^{(3)} + \Omega_{21j}^{(3)})\cos k_j a + (\Omega_{11j}^{(3)} - \Omega_{21j}^{(3)})\sin k_j a\}\psi_{1nj} + \sum_{m=2}^{\infty}\{(\Omega_{1mj}^{(3)} + \Omega_{2mj}^{(3)})\cosh k_{mj} a + (\Omega_{1mj}^{(3)} - \Omega_{2mj}^{(3)})\sinh k_{mj} a\}\psi_{mnj}\right] \tag{39}$$

$$\Lambda_{n4j} = \varphi_{0j}^{-1}\left[-k_j\{(\Omega_{11j}^{(3)} + \Omega_{21j}^{(3)})\sin k_j a - (\Omega_{11j}^{(3)} - \Omega_{21j}^{(3)})\cos k_j a\}\psi_{1nj} + \sum_{m=2}^{\infty} k_{mj}\{(\Omega_{1mj}^{(3)} + \Omega_{2mj}^{(3)})\sinh k_{mj} a + (\Omega_{1mj}^{(3)} - \Omega_{2mj}^{(3)})\cosh k_{mj} a\}\psi_{mnj}\right] \tag{40}$$

where

$$\Psi_{mnj} \equiv \int_h^d f_{mj}(z) g_{nj}(z)\,\mathrm{d}z, \quad n = 1, 2, 3, \ldots$$

APPENDIX II

The vectors and matrices associated with the reflection and transmission coefficients in equations (24a)–(24d), $U_{aj}^{(1)}$, $V_{aj}^{(1)}$, $U_{sj}^{(1)}$, and $V_{sj}^{(1)}$, are expressed as follows.

For antisymmetric parts of the velocity potentials:

$$U_{aj}^{(1)} = \begin{bmatrix} (u_{11j}^{a}+1) & u_{12j}^{a} & \cdots & u_{1(m+1)j}^{a} & u_{1(m+2)j}^{a} & \cdots & u_{1(2m)j}^{a} \\ u_{21j}^{a} & (u_{22j}^{a}+1) & \cdots & u_{2(m+1)j}^{a} & u_{2(m+2)j}^{a} & \cdots & u_{2(2m)j}^{a} \\ \vdots & \vdots & \vdots & \vdots & \vdots & \vdots & \vdots \\ u_{(m+1)1j}^{a} & u_{(m+1)2j}^{a} & \cdots & (u_{(m+1)(m+1)j}^{a}-1) & u_{(m+1)(m+2)j}^{a} & \cdots & u_{(m+1)(2m)j}^{a} \\ u_{(m+2)1j}^{a} & u_{(m+2)2j}^{a} & \cdots & u_{(m+2)(m+1)j}^{a} & (u_{(m+2)(m+2)j}^{a}-1) & \cdots & u_{(m+2)(2m)j}^{a} \\ \vdots & \vdots & \vdots & \vdots & \vdots & \vdots & \vdots \\ u_{(2m)1j}^{a} & u_{(2m)2j}^{a} & \cdots & u_{(2m)(m+1)j}^{a} & u_{(2m)(m+2)j}^{a} & \cdots & (u_{(2m)(2m)j}^{a}-1) \end{bmatrix} \tag{41}$$

$$V_{aj}^{(1)} = \langle 1-(u_{11j}^{a}+u_{1(m+1)j}^{a}) \quad -(u_{21j}^{a}+u_{2(m+1)j}^{a}) \quad \cdots \quad -1-(u_{(m+1)1j}^{a}+u_{(m+1)(m+1)j}^{a}) \\ -(u_{(m+2)1j}^{a}+u_{(m+2)(m+1)j}^{a}) \quad \cdots \quad -(u_{(2m)1j}^{a}+u_{(2m)(m+1)j}^{a})\rangle^{\mathrm{T}} \tag{42}$$

in which

$$u_{pqj}^{a} = \begin{cases} \alpha_{1qj}(\tan k_j c_0 - \mathrm{i}) & \text{for } p=1 \text{ and } q=1,2,\ldots,m \\ \beta_{1(q-m)j}(\tan k_j c_0 + \mathrm{i}) & \text{for } p=1 \text{ and } q=m+1,m+2,\ldots,2m \\ \alpha_{pqj}(\tanh k_{pj} c_0 + 1) & \text{for } p=2,3,\ldots,m \text{ and } q=1,2,\ldots,m \\ \beta_{p(q-m)j}(\tanh k_{pj} c_0 - 1) & \text{for } p=2,3,\ldots,m \text{ and } q=m+1,m+2,\ldots,2m \\ \alpha_{1qj}(\tan k_j c_0 + \mathrm{i}) & \text{for } p=m+1 \text{ and } q=1,2,\ldots,m \\ \beta_{1(q-m)j}(\tan k_j c_0 - \mathrm{i}) & \text{for } p=m+1 \text{ and } q=m+1,m+2,\ldots,2m \\ \alpha_{(p-m)qj}(\tanh k_{pj} c_0 - 1) & \text{for } p=m+2,m+3,\ldots,2m \text{ and } q=1,2,\ldots,m \\ \beta_{(p-m)(q-m)j}(\tanh k_{pj} c_0 + 1) & \text{for } p=m+2,m+3,\ldots,2m \text{ and } q=m+1,m+2,\ldots,2m \end{cases} \tag{43}$$

where $i = \sqrt{-1}$ and

$$\alpha_{1qj} = \frac{k'_j}{2k_j}\cot k'_j a \Psi_{11j}\Psi_{q1j} + \sum_{n=2}^{\infty}\frac{k'_{nj}}{2k_j}\coth k'_{nj} a \Psi_{1nj}\Psi_{qnj}$$

$$\beta_{1qj} = \frac{k'_j}{2k_j}\tan k'_j a \Psi_{11j}\Psi_{q1j} - \sum_{n=2}^{\infty}\frac{k'_{nj}}{2k_j}\tanh k'_{nj} a \Psi_{1nj}\Psi_{qnj}$$

$$\alpha_{pqj} = \frac{k'_j}{2k_{pj}} \cot k'_j a \Psi_{p1j} \Psi_{q1j} + \sum_{n=2}^{\infty} \frac{k'_{nj}}{2k_{pj}} \coth k'_{nj}\, a \Psi_{pnj} \Psi_{qnj}$$

$$\beta_{pqj} = \frac{k'_j}{2k_{pj}} \tan k'_j a \Psi_{p1j} \Psi_{q1j} - \sum_{n=2}^{\infty} \frac{k'_{nj}}{2k_{pj}} \tanh k'_{nj} a \Psi_{pnj} \Psi_{qnj} \tag{44}$$

in which $\Psi_{pqj} \equiv \int_h^d f_{pj}(z) g_{qj}(z)\, \mathrm{d}z$.

For symmetric parts of the velocity potentials:

$$U_{sj}^{(1)} = \begin{bmatrix} (u^s_{11j}+1) & u^s_{12j} & \cdots & u^s_{1(m+1)j} & u^s_{1(m+2)j} & \cdots & u^s_{1(2m)j} \\ u^s_{21j} & (u^s_{22j}-1) & \cdots & u^s_{2(m+1)j} & u^s_{2(m+2)j} & \cdots & u^s_{2(2m)j} \\ \vdots & \vdots & \vdots & \vdots & \vdots & \vdots & \vdots \\ u^s_{(m+1)1j} & u^s_{(m+1)2j} & \cdots & (u^s_{(m+1)(m+1)j}-1) & u^s_{(m+1)(m+2)j} & \cdots & u^s_{(m+1)(2m)j} \\ u^s_{(m+2)1j} & u^s_{(m+2)2j} & \cdots & u^s_{(m+2)(m+1)j} & (u^s_{(m+2)(m+2)j}+1) & \cdots & u^s_{(m+2)(2m)j} \\ \vdots & \vdots & \vdots & \vdots & \vdots & \vdots & \vdots \\ u^s_{(2m)1j} & u^s_{(2m)2j} & \cdots & u^s_{(2m)(m+1)j} & u^s_{(2m)(m+2)j} & \cdots & (u^s_{(2m)(2m)j}+1) \end{bmatrix} \tag{45}$$

$$V_{sj}^{(1)} = \langle 1 - (u^s_{11j} + u^s_{1(m+1)j}) \quad -(u^s_{21j} + u^s_{2(m+1)j}) \quad \cdots \quad -1 - (u^s_{(m+1)1j} + u^s_{(m+1)(m+1)j}) \\ -(u^s_{(m+2)1j} + u^s_{(m+2)(m+1)j}) \quad \cdots \quad -(u^s_{(2m)1j} + u^s_{(2m)(m+1)j}) \rangle^{\mathrm{T}} \tag{46}$$

in which

$$u^s_{pqj} = \begin{cases} \beta_{1qj}(\cot k_j c_0 + \mathrm{i}) & \text{for } p=1 \text{ and } q=1,2,\ldots,m \\ \alpha_{1(q-m)j}(\cot k_j c_0 - \mathrm{i}) & \text{for } p=1 \text{ and } q=m+1,m+2,\ldots,2m \\ \beta_{pqj}(\coth k_{pj} c_0 + 1) & \text{for } p=2,3,\ldots,m \text{ and } q=1,2,\ldots,m \\ \alpha_{p(q-m)j}(\coth k_{pj} c_0 - 1) & \text{for } p=2,3,\ldots,m \text{ and } q=m+1,m+2,\ldots,2m \\ \beta_{1qj}(\cot k_j c_0 - \mathrm{i}) & \text{for } p=m+1 \text{ and } q=1,2,\ldots,m \\ \alpha_{1(q-m)j}(\cot k_j c_0 + \mathrm{i}) & \text{for } p=m+1 \text{ and } q=m+1,m+2,\ldots,2m \\ \beta_{(p-m)qj}(\coth k_{pj} c_0 - 1) & \text{for } p=m+2,m+3,\ldots,2m \text{ and } q=1,2,\ldots,m \\ \alpha_{(p-m)(q-m)j}(\coth k_{pj} c_0 + 1) & \text{for } p=m+2,m+3,\ldots,2m \text{ and } q=m+1,m+2,\ldots,2m \end{cases} \tag{47}$$

The vectors and matrices $U_{aj}^{(3)}$, $V_{aj}^{(3)}$, $U_{sj}^{(3)}$, and $V_{sj}^{(3)}$ can be obtained by replacing c_0 with b_0 in equations (43) and (47).

REFERENCES

1. R. D. Hanson, 'Behaviour of liquid storage tanks', in *The Great Alaska Earthquake of 1964*, National Academy of Science, Washington, DC, 1973, pp. 331–339.
2. P. E. Jennings (ed.), 'Engineering features of the San Fernando earthquake of Feb 9, 1971', *EERL-71-02*, California Institute of Technology, 1971, pp. 434–470.

3. G. C. Manos and R. W. Clough, 'Tank damage during the May 1983 Coalinga, California earthquake', *Earthquake Engng. Struct. Dyn.* **13**(4), 1985, pp. 449–466.
4. R. Nielsen and A. S. Kiremidjian, 'Damage to oil refineries from major earthquakes', *J. Struct. Engng. ASCE* **112**(6), 1986, pp. 1481–1491.
5. C. F. Shih and C. D. Babcock, 'Buckling of oil storage tanks in SPPL tank farm during the 1979 Imperial Valley earthquake', *J. Press. Vessel Technol. ASME* **109**(2), 1987, pp. 249–255.
6. G. C. Manos, 'Evaluation of the earthquake performance of anchored wine tanks during the San Juan, Argentina, 1977 earthquake', *Earthquake Engng. Struct. Dyn.* **20**(12), 1991, pp. 1099–1114.
7. M. A. Haroun, S. A. Mourad and W. Izzeddine, 'Performance of liquid storage tanks during the 1989 Loma Prieta earthquake', *Proc. Lifeline Earthquake Engng*, Los Angeles, ASCE, 1991, pp. 1152–1160.
8. T. W. Cooper, 'A study of the performance of petroleum storage tanks during earthquakes 1933–1995', *NIST GCR 97-720*, National Institute of Standards and Technology, 1991.
9. A. S. Veletsos, 'Seismic response and design of liquid storage tanks', in *Guidelines for the Seismic Design of Oil and Gas Pipeline Systems*, Tech. Council on Lifeline Earthquake Engineering, ASCE, New York, 1984, pp. 255–364.
10. A. Huerta, W. K. Liu and J. Gvildys, 'Large amplitude sloshing with submerged blocks', *Sloshing and Fluid Structure Vibration-1989*, ASME PVP Conference, Honolulu, Hawaii, PVP Vol. 157, 1989, pp. 143–148.
11. H.-M. Koh, J. Kim and J.-H. Park, 'Seismic analysis of rectangular liquid storage structure with submerged objects by a coupled finite element-boundary element method', *Trans. 13th Int. Conf. on Structural Mechanics in Reactor Technology*, Porto Alegre, Brazil, Division K, 1995, pp. 323–334.
12. K. Tai, T. Nakatogawa, T. Hisada and H. Kawakami, 'Numerical study on fluid-submerged block interaction in water pool', *Trans. 13th Int. Conf. on Structural Mechanics in Reactor Technology*, Porto Alegre, Brazil, Division K, 1995, pp. 469–474.
13. Y.-S. Kim and C.-B. Yun, 'A spurious free four-node displacement-based fluid element for fluid–structure interaction analysis', *Engng. Struct.* **19**(8), 1997, pp. 665–678.
14. D. C. Ma and Y. W. Chang, 'Analysis of seismic sloshing of reactor tanks considering submerged components and seismic isolation', *Proc. ASME PVP Conf.*, New Orleans, June 23–26, PVP Vol. 98-7, 1985, pp. 139–147.
15. D. C. Ma, J. Gvildys and Y. W. Chang, 'Effects of deck-mounted components on the sloshing response of a pool-type LMFBR', *Trans. 8th Int. Conf. on Structural Mechanics in Reactor Technology*, Brussels, Belgium, Vol. E, 1985, pp. 31–36.
16. A. Sakurai, Y. Masuko, C. Kurihara, K. Ishihama, T. Yashiro, Y. W. Chang and E. Rodwell, 'Seismic sloshing experiments of large pool-type fast breeder reactors', *Nucl. Engng. Des.* **113**(3), 1989, pp. 423–433.
17. Y. W. Chang, J. Gvildys, D. C. Ma, R. Singer, E. Rodwell and A. Sakurai, 'Numerical simulation of seismic sloshing of LMR reactors', *Nucl. Engng. Des.* **113**(3), 1989, pp. 435–454.
18. Y.-S. Choun, 'Sloshing analysis of rectangular fluid–structure systems with a submerged structure for seismic loading', *Ph.D. Dissertation*, Korea Advanced Institute of Science and Technology, Taejon, Korea, February 1998.
19. D. Fischer, 'Dynamic fluid effects in liquid-filled flexible cylindrical tanks', *Earthquake Engng. Struct. Dyn.* **7**(6), 1979, pp. 587–601.
20. H. Parkus, 'Modes and frequencies of vibrating liquid-filled tanks', *Int. J. Engng. Sci.* **20**, 1982, pp. 319–326.
21. M. A. Haroun, 'Vibration studies and tests of liquid storage tanks', *Earthquake Engng. Struct. Dyn.* **11**(2), 1983, pp. 179–206.
22. C. C. Mei and J. L. Black, 'Scattering of surface waves by rectangular obstacles in waters of finite depth', *J. Fluid Mech.* **38**, 1969, pp. 499–511.
23. J. N. Newman, 'Propagation of water waves past long two-dimensional obstacles', *J. Fluid Mech.* **23**, 1965, pp. 23–29.
24. R. Porter and D. V. Evans, 'Complementary approximations to wave scattering by vertical barriers', *J. Fluid Mech.* **294**, 1995, pp. 155–180.
25. Y.-S. Choun and C.-B. Yun, 'Sloshing characteristics in rectangular tanks with a submerged block', *Comput. Struct.* **61**(3), 1996, pp. 401–413.
26. R. W. Clough and J. Penzien, *Dynamics of Structure*, 2nd edn, McGraw-Hill, New York, 1993.

